SSME MAIN COMBUSTION CHAMBER AND NOZZLE FLOWFIELD ANALYSIS

Final Report, Contract No. NAS8-35510

CI-FR-0085

Prepared for:

National Aeronautics and Space Administration
George C. Marshall Space Flight Center
Marshall Space Flight Center, AL 35812

Prepared By:
Richard C. Farmer
Ten-See Wang
Sheldon D. Smith
Robert J. Prozan

CONTINUUM, INC.
4715 University Drive, Suite 118
Huntsville, AL 35816-3495

SSME MAIN COMBUSTION CHAMBER AND

NOZZLE FLOWFIELD ANALYSIS

Final Report, Contract No. NAS8-35510
Report Number - CI-FR-0085

Prepared for:

National Aeronautics and Space Administration
George C. Marshall Space Flight Center
Marshall Space Flight Center, AL 35812

Prepared By:
Richard C. Farmer
Ten-See Wang
Sheldon D. Smith
Robert J. Prozan

CONTINUUM, INC.
4715 University Drive, Suite 118
Huntsville, AL 35816-3495

March 1, 1986

TABLE OF CONTENTS

TABLES/ FIGURES

1. INTRODUCTION

Steady flow in the main combustion chamber and nozzle of a large axisymmetric rocket motor, such as the SSME, is generally well understood. Analytical treatments of transient phenomena have previously been insufficient to quantitatively evaluate unsteady pressure and heating loads. Three-dimensional steady and transient combustion chamber/nozzle flows have, in the past, been computationally modeled in a rudimentary fashion. Performance losses in a rocket engine which are flow related consist of boundary layer, (both thermal and fricitional), streamline curvature, non-uniform mixture ratios, and phase and chemical kinetics. All of these phenomena have been isolated for analytical study. Since the development of Navier-Stokes and turbulence solvers, all of the flow phenomena may be directly addressed. Furthermore, transient flows may also be simulated. This investigation is an initial attempt at unified flow analysis of the gas dynamics of these flow processes.

Steady operating pressure is reached in about four seconds in the SSME. The relatively slow chamber pressure buildup in the SSME makes it possible to treat the operation as a series of quasi steady solutions with variable chamber pressures until steady operating conditions are reached. At reduced chamber pressures the nozzle is may be only partially filled with exhaust gases resulting in a separated flow region between the main exhaust stream and the nozzle wall. Similar flow conditions existed in ground level static tests of the J-2, and were the probable cause of the teepee flow structure observed in those tests.

This research study was an investigation of the computational fluid dynamics tools which would accurately analyze main combustion chamber and nozzle flow. The importance of combustion phenomena and local variations in mixture ratio are fully appreciated; however, the computational aspects of the gas dynamics involved were the sole issues addressed in this study. The CFD analyses made are first compared with conventional nozzle analyses to determine the accuracy for steady flows, and then transient analyses are discussed.

2. STEADY FLOW PREDICTIONS

Steady, axisymmetric flowfield analyses for the flows in liquid rocket engines have been available for many years (Ref. 1,2). The direct solution of the governing conservation equations without making multiple analyses of the various flowfield substructures could not be accomplished until computers of sufficient size and speed and Navier-Stokes/turbulent flow solvers were developed. This investigation was an assessment of Continuum's VAST code (Ref. 3), a Navier-Stokes solver, as a transient model for SSME main combustion chamber/nozzle flowfield predictions. Boundary condition treatments and model verifications are presented in this report.

2.1 Transonic Solution

One of the components of the main combustion chamber and nozzle flow analysis is the combustion chamber and transonic flow analysis. Prior to this contract, the applicability of the VAST code to mixed (subsonic-transonic-supersonic)internal flows had not been adequately demonstrated. Thus, the immediate application of the VAST code to the main combustion chamber-nozzle transonic solution was not undertaken until a validation calculation was performed. Generally, code validation is performed by comparing a calculation against either experimental data or an accepted model's calculations. In the late 60's L. Back (Ref. 4) of Jet Propulsion Laboratory performed an experimental study of a small throat radius of curvature ratio, converging, diverging nozzle. The experimental nozzle flowed room temperature air. High resolution data was taken on the nozzle wall and centerline which provided Mach numbers and static pressure distributions. Good comparison with this data is considered an important check on any candidate nozzle analysis.

The geometry of Back's nozzle is shown in Fig. 1. The nozzle is a converging diverging nozzle with a throat radius of .8 in., a contraction area ratio of 9.76, an expansion area ratio of 6.6, a 45 deg. inlet angle, a radius of curvature ratio of 1 from the combustion chamber to inlet and a throat radius of curvature ratio of .625. The problem was set up using four regions, A total of 780 grid points were used. There were 15 points in the lateral direction and axially: 12 (region 1), 15 (region 2), 8 (region 3) and 17 (region 4). The first region extended .6 in. upstream of the entrance to allow the flow to stabilize at

the real entrance. The first region went from -.6 to .881 in. with two segments. The first segment of region 1 is a straight line from -.6 to .315 having a constant radius of 2.5 inc. The second segment consisted of a .8 in. radius circular arc whose center is at X= .315 and R =6.7. The second region is the inlet to the throat at - 45 deg., having 15 points axially. Region 3 consists of eight axial points described by a circular arc whose radius is .5 in. and extends from the - 45 deg. inlet to the 15 deg. conical expansion section. The center of the circular arc is at X = 2.554, R = 1.3 and extends for X=2.2 to 2.683. The fourth region is described by a 15 deg. cone extending to an X of 5.6 in.. The resulting grid is shown in Fig. 2.

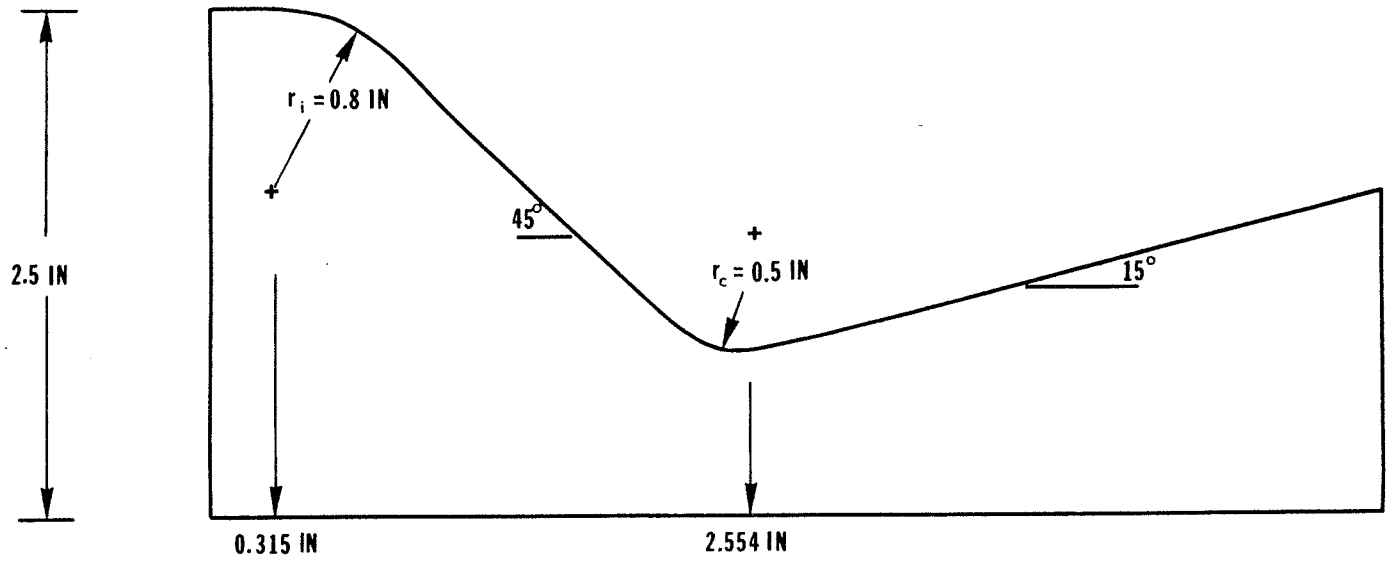

Fig. 1 The Geometry of Back's Nozzle

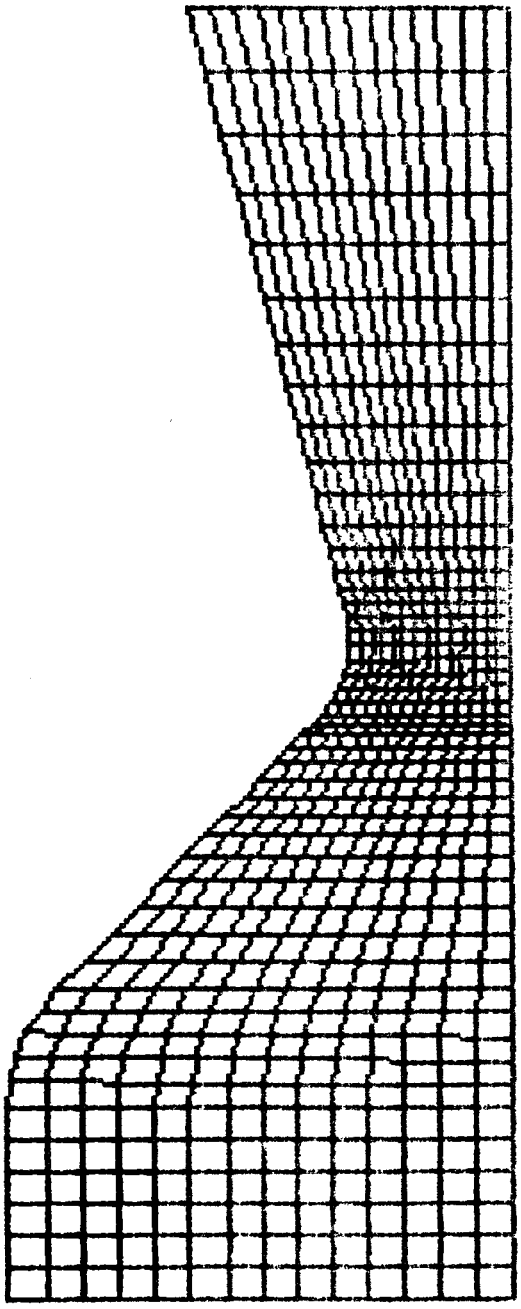

Fig. 2 VAST Grid for Back's Nozzle

Boundary conditions which were imposed on Back's nozzle were tangency for the combustion chamber/nozzle wall and axis, free conditions on the exit and total conditions at the inlet. Total conditions for Back's nozzle were 150.0 psia chamber pressure and 540 R chamber temperature.

The results of the VAST prediction of Back's nozzle are shown in Fig. 3 and 4. Figure 3 presents a comparison of VAST and experimental static pressure distributions along the combustion chamber/nozzle wall and centerline. Figure 4 presents the same comparison for Mach number. As can be seen from these two figures, the comparison between VAST and the data is excellent. The only small deviation occurs at the recompression region downstream of the throat. By adding additional grid points in this region, the match would be much better.

The applicability of the VAST code to solve mixed (subsonic-transonic-supersonic) type flows which occur in rocket engine combustion chamber and nozzles has been verified through a comparison with experimental data. The VAST code can now confidently be used to solve the SSME combustion chamber/nozzle and other liquid rocket engines.

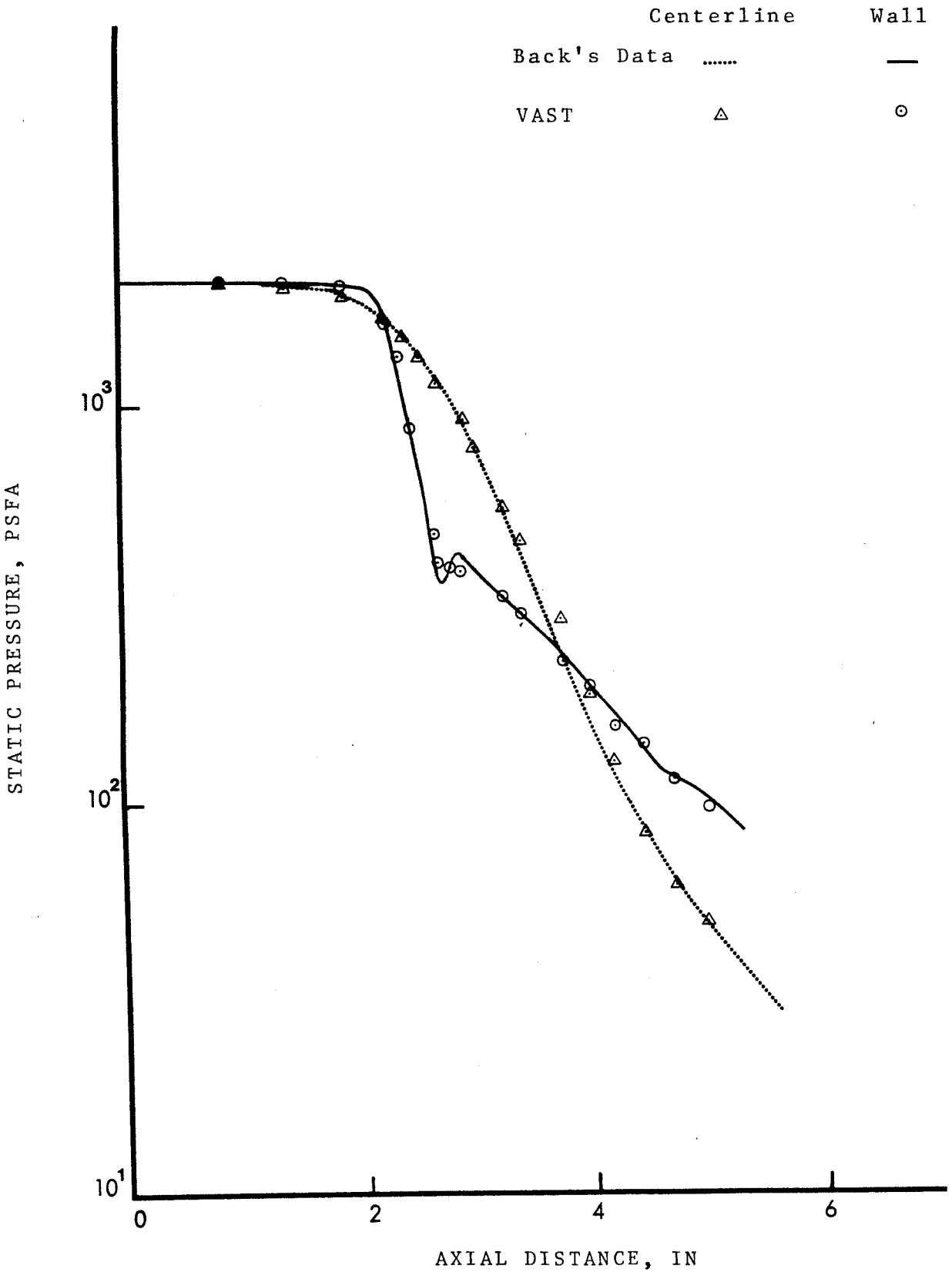

Fig. 3 Back's nozzle centerline and wall static pressure distribution

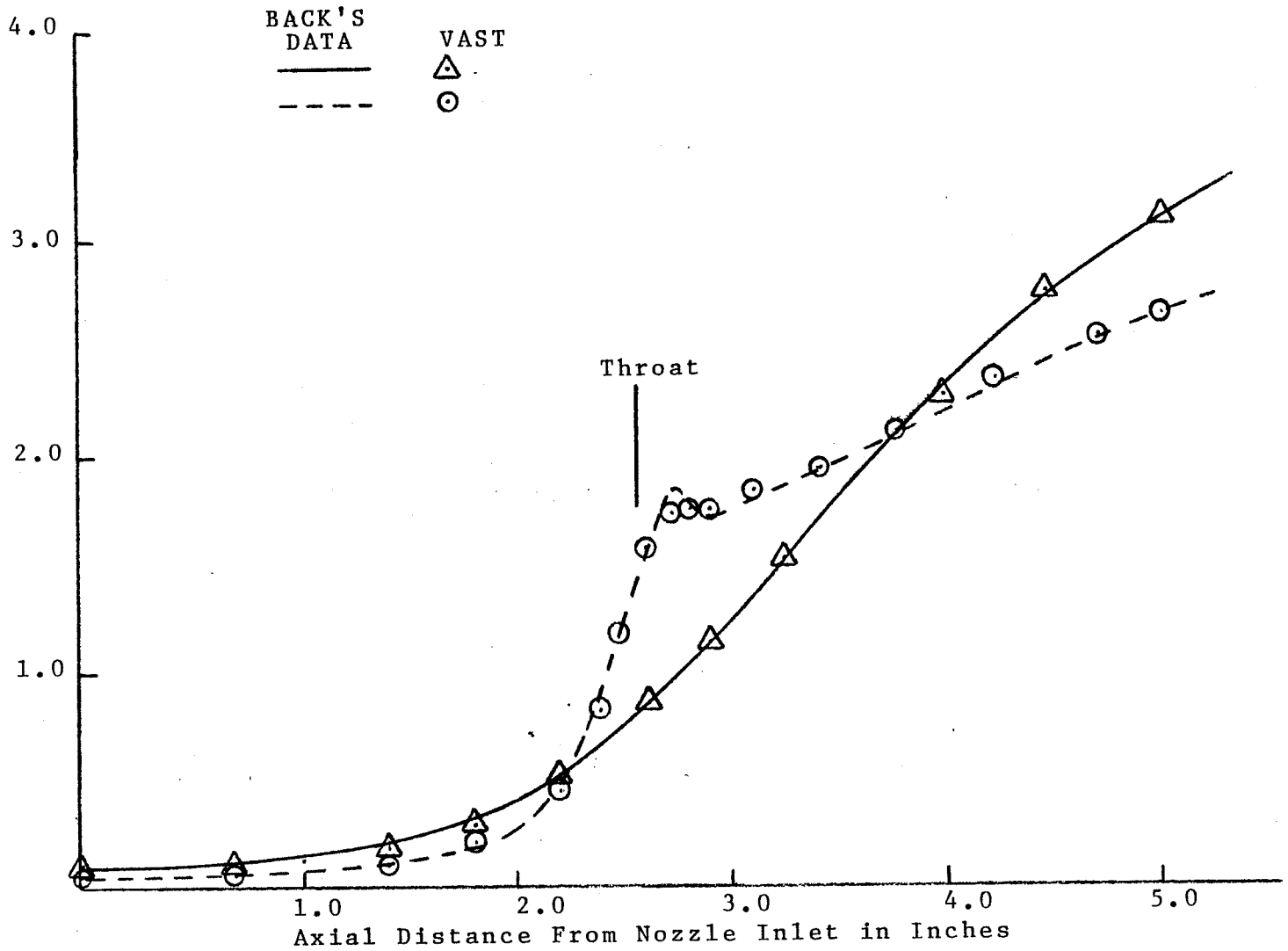

Fig. 4 Back's Nozzle Mach Number Distributions

2.2 Inviscid Nozzle Expansions

Expansions in propulsion nozzles are routinely analyzed by using a method of characteristics (MOC) program followed by a calculation of the nozzle boundary layers (Ref. 5). The inviscid predictions by the VAST code were tested by comparison to MOC predictions for ideal gas expansion in the SSME nozzle geometry for a specified sonic line boundary condition. The results of this investigation are reported in this section.

Initial predictions with the VAST code for a relatively crude grid had excellent wall property comparisons, but failed to predict the rapid centerline expansions known to be present in the nozzle. The accuracy, as reflected by increasing the grid density, and the effect of downstream boundary conditions on pressure were investigated as a means of improving the centerline flow properties. Neither of these effects improved the predictions. The manifestation of the error was that total pressure deviated from the known value when the expansion became large, i.e. several orders of magnitude decrease in static pressure during the expansion. This is a well known problem in using direct solutions of the Euler equations for nozzle flows, as was recently reconfirmed in (Ref. 6, 7). The VAST code was modified to check and reset the mechanical energy and total energy at each computation step. Results of these calculations are shown in Figs. 5 and 6. Centerline and wall values of pressure and Mach number are shown to be accurately predicted for the coarse grid calculation. The VAST code was modified to perform the integrations required to predict performance, these results are shown in Table 1. Thrust was predicted to be within 0.5 percent of the value obtained from the MOC calculation and mass flow at the exit was calculated to be within 0.2 percent of that specified at the throat. The mass flow conservation of the coarse grid VAST calculation is better than that obtained in the MOC prediction. Since the MOC is a hyperbolic marching solution while VAST is an elliptic solver, the VAST solution for the steady inviscid nozzle flow obviously required longer computation time than the MOC solution did. The use of the constant mechanical energy and total energy creates problems if viscous/turbulent flows or unsteady flows are considered. These issues are addressed subsequently. In summary, accurate, steady, inviscid, large expansion nozzle flows are predicted for even coarse-grid, supersonic nozzle expansions.

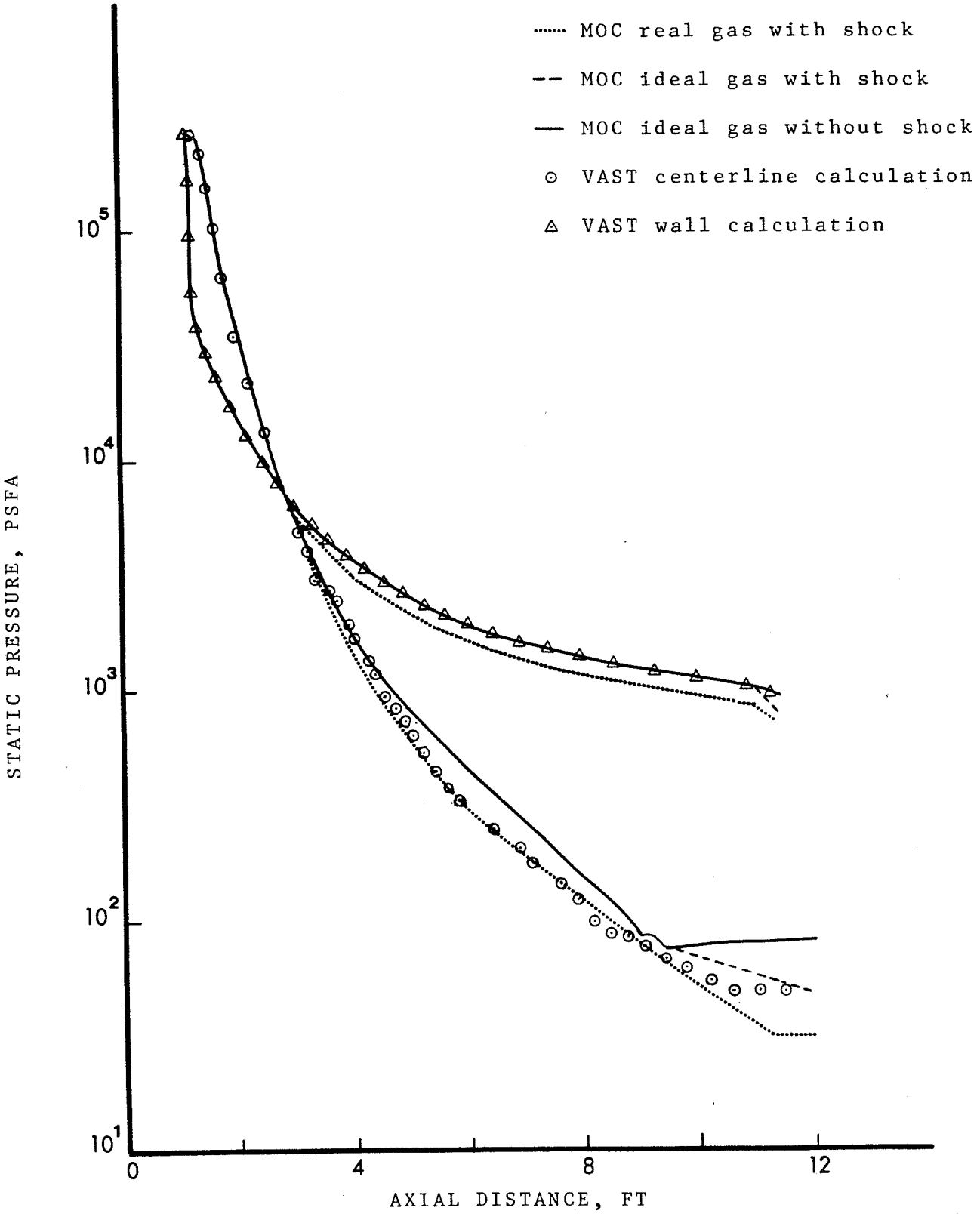

Fig. 5 SSME nozzle centerline and wall static pressure distribution

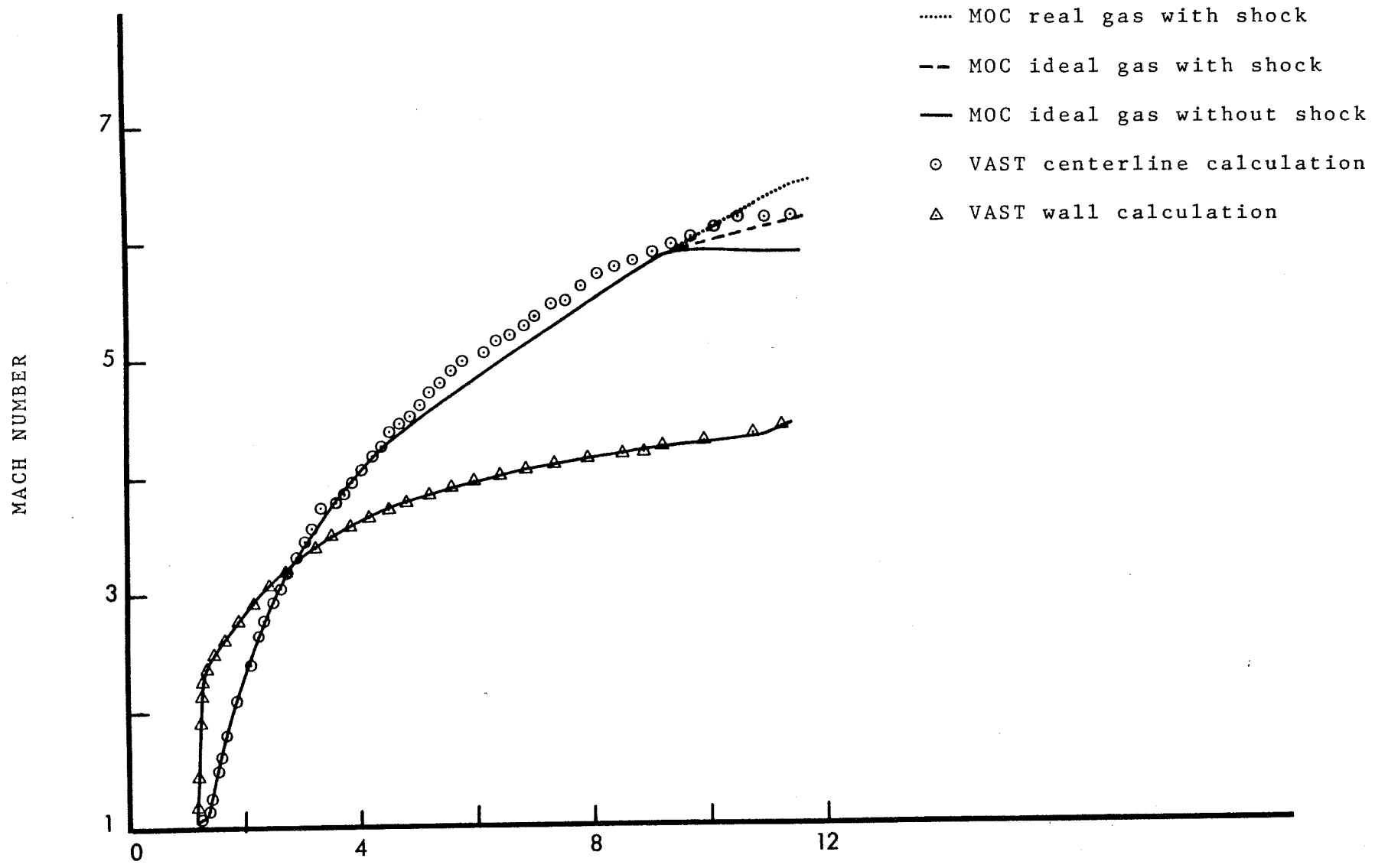

Fig. 6 SSME nozzle centerline and wall Mach number distribution

Table 1

PERFORMANCE PREDICTIONS

	MOC	VAST
mass flowrate		
o at the throat	1119	1119
o at the exit	1109	1117
axial momentum at the throat, plus the wall pressure integral normalized by the mass flowrate	518.1	520.9

NOTE: The table values are for an ideal gas with an arbitrary sonic line used as a startline. They are for comparison only; actual values for the SSME are different than the table values.

2.3 Turbulence Effects

Models to represent the turbulent exchange of momentum and energy must be postulated to close the time averaged conservation equations. These models should be included in the calculational procedure. Since the phenomena cannot be predicted from fundamental principles, either experimental data or analogies to more simple flows must be used to treat complex turbulent flows like those within the SSME combustion chamber and nozzle. The time scale for the turbulence averaging is presumed to be less than the time scale of interest in transient predictions.

2.3.1 Turbulence Models

Turbulent flow causes enhanced mixing and, in some instances, convective-like flow which is superimposed on an inviscid flow field. Four general types of models are currently used to represent turbulent flows. The first three of these models start with the time averaged conservation equations:

1. Algebraic eddy viscosity models.
2. One- and two-equation models.
3. Full Reynolds-stress models.
4. Distribution function models.

For flows in which some of the turbulence scales are much larger than those for other important flow phenomena, distribution function models have been used. None of these turbulence models are predictive, all require experimentally determined parameters as input. Flows over plates and in pipes are the only ones for which even a reasonably complete data base is available; however, the behavior of turbulence models in predicting flows around cylinders and over back steps must be reasonable for the models to be generally useful.

Factors affecting the type of prediction required and/or the geometric and vorticial complexity of the flow must also enter into the selection of the turbulence model used. Of necessity the computational algorithm, employed for a given CFD analysis, utilizes a particular grid density. The selected grid density may require the use of auxiliary boundary conditions to obtain an accurate solution. These additional boundary conditions

are generally referred to as "wall functions." The nature of wall functions and the manner in which they are utilized varies greatly from one investigation to another. The use of wall functions per se does not rule out the possibility of describing heat transfer effects or flow reversal in zones of separated flow. On the other hand, no general-purpose, well-established set of wall functions currently exists.

Currently available turbulence data and flow models are summarized and a model for describing engine related flows is then presented.

2.3.2 Turbulent Wall Flow Data and Correlations

Turbulent flows in smooth pipes and over smooth flat plates have been measured extensively. Typical data are shown in Fig. 7. Although the velocity changes very rapidly close to the wall, its variation has been measured. These data are well represented, piecewise, with the first three equations in Fig. 8 for plates without pressure gradients and for pipes. Data in the outer region are better fit for plate flow with pressure gradients by the fourth equation in Fig. 8.

In order to calculate velocity gradients from empirical velocity profiles, it is beneficial to represent velocity as a continuous function of distance from the wall. Such a correlation is shown in Fig. 9. Correlations for wall shear stress and boundary layer thickness as functions of free-stream conditions and/or average flow conditions have also been developed.

The most elementary representation of turbulent flow is to postulate an eddy viscosity by analogy to laminar viscosity whereby shear stress is determined as the product of eddy viscosity times the velocity gradient (the Boussinesq approximation). Measurements of eddy viscosity have been made as shown in Figure 10. To relate eddy viscosity to mean turbulent flow profies, two new pieces of information are required: the values of shear stress and of velocity gradient as functions of position from the wall. For fully developed pipe flow $\tau_{rx} = \tau_w (1-y/R)$. Experimental shear stress data for flow over a flat plate are shown in Fig. 11; note the profiles are approximately equal.

Assuming a logarithmetic velocity profile

$$u = (u_\tau/\kappa) \ln y + \text{constant}$$

$$\frac{\partial u}{\partial y} = (u_\tau/\kappa y)$$

$$\mu_e = u_\tau \rho (1-y/R) \kappa y$$

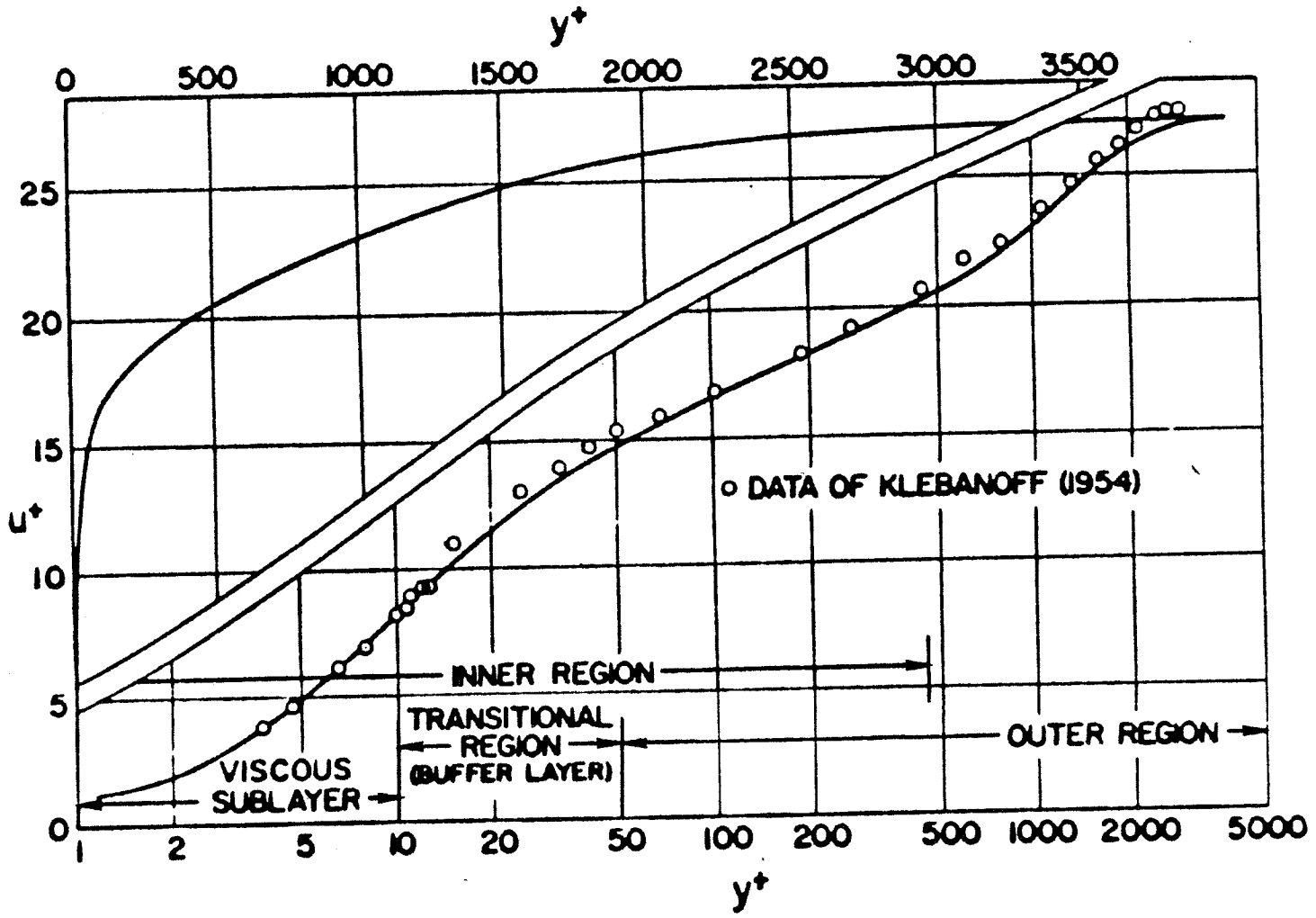

Fig. 7 Semilogarithmic and linear plots of mean velocity distribution across a turbulent boundary layer with zero pressure gradient

Empirical.

$$u^+ = u/u_\tau = y\ u_\tau/\nu \equiv y^+ \qquad 0 < y^+ < 5$$

$$u^+ = (2/\kappa)\ \ln(y^+) - 3.05 \qquad 5 < y^+ < 30$$

$$u^+ = (1/\kappa)\ \ln(y^+) + B \qquad 30 < y^+ < 500$$

$$(\kappa,\ B) = (0.4,\ 5.5)_N = (0.41,\ 5.0)_C \text{ for plates \& pipes}$$

$$\frac{U_e - u}{u_\tau} = -\ (1/\kappa)\ \ln(y/\delta) + A \qquad 50 < y^+$$

A varies for pipes, flat plates & flows w/pressure gradients

Fig. 8 Velocity profiles for pipes and flat plates

$$(u/u_\tau) = 5.424 \tan^{-1}(0.1198\ y^+ - 0.4880) - 3.52$$

$$+ 4.168 \ln(y^+ + 10.6) - 0.8684 \ln(y^{+2} - 8.15\ y^+ + 86)$$

$$+ (14.64\ \Pi + 2.44)(y/\delta)^2 - (9.76\ \Pi + 2.44)(y/\delta)^3$$

when $u_\tau = (\tau_w/\rho)^{0.5}$

$\Pi = \kappa\ A/2$, A = 2.35 flat plate

A = 0.65 pipes

$\Pi = 0.8\ (\beta + 0.5)^{0.75}$

$\beta = (\delta^*/\tau_w)(dP/dx)$

Fig. 9 Musker's equation for velocity as a function of distance from the wall

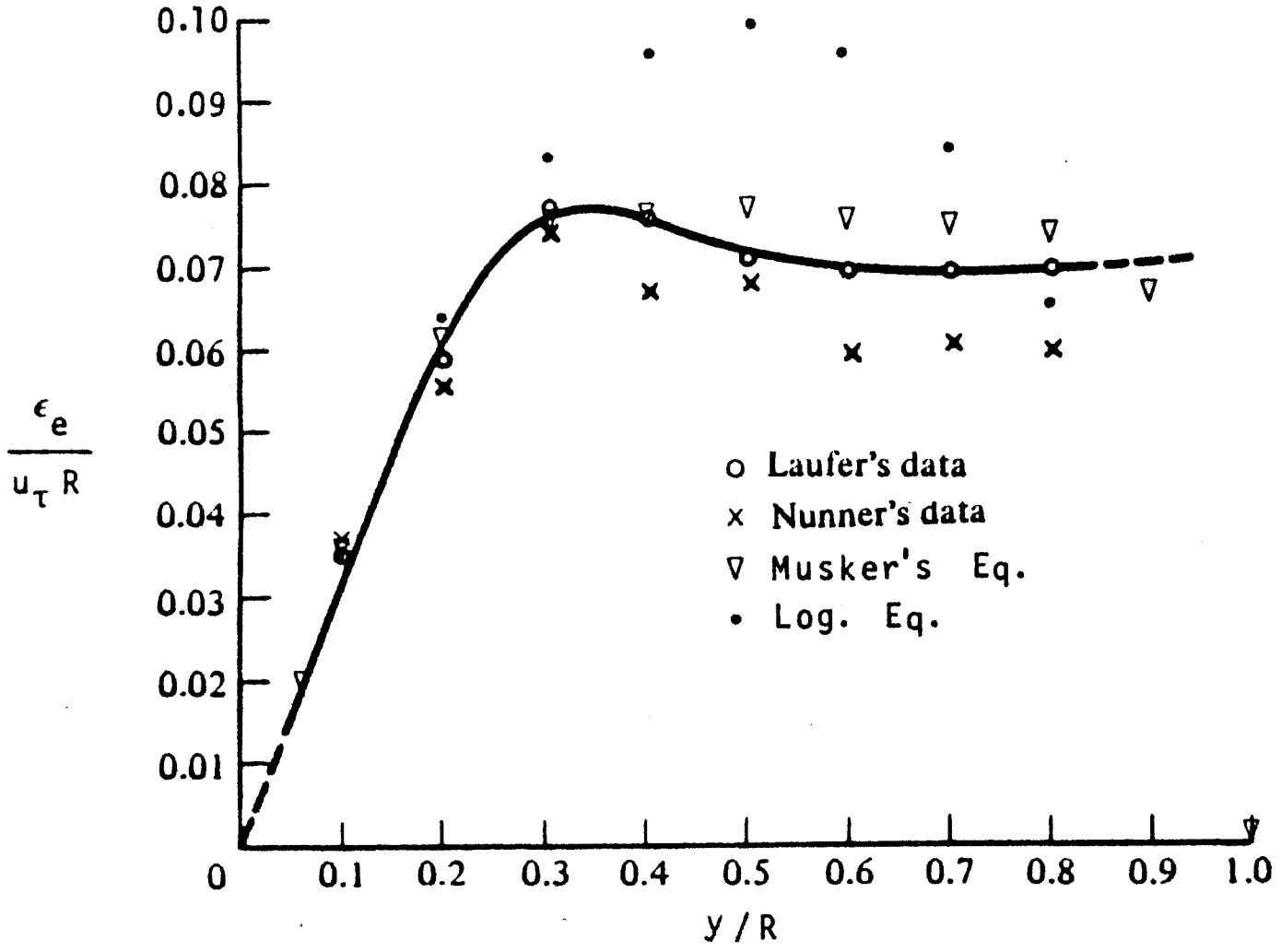

Fig. 10 Eddy viscosity in pipe flow

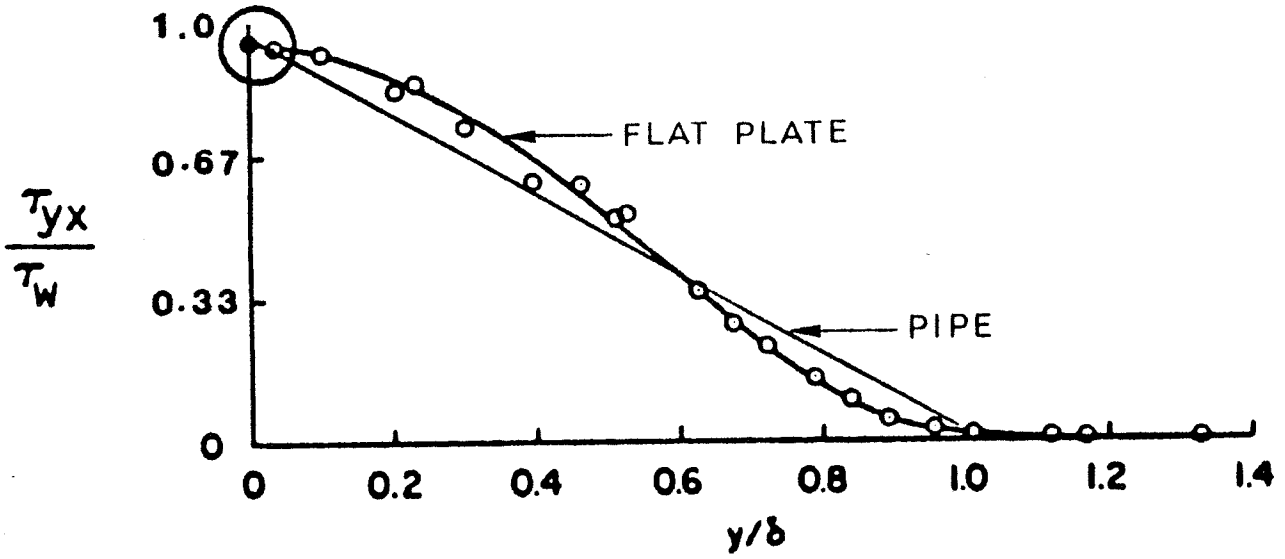

Fig. 11 Dimensionless shear-stress distribution across the boundary layer at zero pressure gradient, according to the data of Klebanoff (1954)

This value of eddy viscosity is plotted in Fig. 10. Notice that excellent agreement is obtained for the 30 percent of the flow nearest the wall. If a better velocity profile is used, a better fit of μ_e should be obtained. Such is the case shown in Fig. 10 where Musker's correlation from Fig. 9 is used. The friction velocity, u_τ, may be evaluated with a Reynolds-number/friction-factor correlation, thusly:

$$\frac{\mu_e}{\mu} = (1-y/R)\ (\kappa/2R)\ \left(\frac{u_\tau}{V}\right)\ \left(\frac{VD}{\nu}\right)$$

$$\frac{\mu_e}{\mu} = \left(\frac{\kappa y}{2R}\right)\ (1-y/R)\ (Re)\ (f_m/8)$$

Similar correlations exist for flow over a plate; however, an empirical boundary layer thickness equation is required as the length scale to replace the pipe diameter.

Recognizing that analyses of more general flows are also required, a computational technique for the plate and pipe type flows will be developed first. The computational method thus developed will be used as a starting point for more complex flows.

2.3.4 Turbulent Flow Calculation Procedure

Conceptually, a turbulent flow calculation can be made just like a laminar flow, once an eddy viscosity model, or other flow model, is specified. However, the very large velocity gradients near the wall as shown in Fig. 7 indicate that a very fine computational grid would be required to satisfy a no-slip wall condition and to accurately calculate the sharp velocity gradients near the wall. To avoid such computational complexity for so small a region of the flow, a more physical model of the wall region is required. Zero and modest pressure gradient flows over smooth walls yield time-average velocity profiles near the wall which are the same. Since the near wall flows are similar, outer flows will be calculated directly from the solution of the momentum equations and extrapolated from correlation equations near the wall. The empirical equations will be used to evaluate the wall shear stress and the shear stress and velocity gradients at a point located a y^+ of 30 (or slightly more). The near wall point is selected to be $30 < y^+ < 500$ so that the third equation in Fig. 8 and its derivative may be used as the wall functions

for this flow. By assuming negligible flow between the wall and the near wall point, the exact value of y is immaterial, provided only that y^+ remains in the specified bounds. Computationally, this procedure has proved very acceptable. Had the selection of y proved to be very sensitive to flow conditions, a more general empirical velocity correlation, such as Musker's equation, could have been used. To model flows over rough walls, a modification to the empirical equation is made by defining $y^+=y/k_s$ and B=8.5 where k_s is the roughness height. If the walls are not completely rough, $B = fn(u_\tau, k_s, \nu)$ as shown in Schlichting, 7th ed., p. 620 (Ref. 10). If the wall surfaces were roughened with cut grooves rather than random roughness elements, the k_s and B values would be evaluated by fitting test data. In summary, a method of predicting momentum exchange in turbulent wall flows has been presented; subsequent discussion will describe the accuracy of this model.

If empirical temperature correlations were available, all functions could be established for wall heat transfer. Most attempts to generate temperature correlations have used turbulent Prandlt numbers; none of these attempts have resulted in even moderately general correlations. The work of Weigand and Walker (Ref. 11) abandoned the turbulent Prandlt number concept and produced a useful correlation. Their empirical correlation contains more parameters than are needed to fit the modest data base which is available. Physically, the parameters represent streaking and bursting phenomena; however, if such parameters are approximated to represent the available data base only, the correlation equation for temperature becomes that shown in Fig. 12.

Conceptually, either q_w or T_w can be specified, as either constants or as functions of position on the surface, to solve a convective heating problem. To complete the solution, a thermal analysis of the wall is required so that surface heat balances can be made. Assuming T_w is known, or can be calculated, the solution procedure is to calculate the temperature gradient normal to the wall by

$$\left(\frac{\partial T}{\partial y^+}\right)_{30} = \frac{T - T_w}{y^+_{30}} \left(\frac{u_\tau^2}{\kappa_\Theta V \nu_w}\right)$$

at $y^+ = 30$ $(= y^+_{30})$ and use this value as the wall function for temperature. If q_w is to be specified, κ_θ and St are calculated from the equations in Fig. 12, then T_w is calculated for the given q_w and the remainder of the calculation procedes as for the specified T_w case.

TEMPERATURE PROFILES

$$\theta\ (\kappa/u_\tau) = \ln\left\{\frac{2\ y^+\ Pr^{0.5}}{\theta\ (T_r - 1) + 2}\right\} + 9.3027\ Pr^{0.5}\ \kappa_\theta$$
$$- 1.7556 - \exp(-(9.737\ Pr^{0.5}\ \kappa_\theta + 0.6807))$$

where $\theta = (T - T_w)/(T_e - T_w)$

$$T_r = T_e\ /\ T_w$$

$$\kappa_\theta = \kappa\ St\ /\ (u_\tau^2\ T_e\ /\ T_w)$$

$$St = q_w\ /\ \rho_e\ C_p\ U_e\ (T_w - T_e)$$

$$q_w = -\ k_w\ (\partial T/\partial y)_w$$

Note: The denominator of the ln term is a density correction to y^+; such a correction also applies to the compressible velocity correlation equations.

Fig. 12 The correlation equation for temperature

A boundary layer calculation was made for the case shown in Fig. 13. The outlet velocity profile for only 16 nodes in the boundary layer gives a very acceptable solution. A similar case was run for heating to a cold wall and reasonable temperature profiles were obtained. Pressure was held constant for the non-isothermal case to stabilize the solution. In more complex flows, such that the inviscid flow establishes the pressure field, additional stabilization is not required.

To describe geometrically complex flows, the turbulence models just presented are generalized by making the following modifications. The time averaged velocities at points very near the wall are tangent to the wall for flows with no mass addition. For flow on a flat plate there is only one significant shear stress component, whereas for laminar flow in a Cartesian coordinate system all six of the stress components in Table 2 may be important. Since turbulence models for compressible flow have not been well established, μ_2 will be assumed zero for turbulent flows. The velocity gradient determined from the logarithmetic profile described previously will be modified in two ways in order to evaluate the turbulent counterparts of the stress terms in Table 2. Symbolically, this gradient is $d|\bar{V}|/dn$, where n is along a surface normal direction. Direction cosines will convert this gradient into components along the coordinate directions.

$$(d|\bar{V}|/dn)(BCX_i) = d(V)/dx_i$$

Then velocity components will be considered.

$$(d|V|/dx_i)(V_j/|V|) = dV_j/dx_i$$

Hence, all of the shear stress terms can be evaluated for arbitrarily oriented surfaces.

Velocity and temperature for SSME type nozzle flows were also computed and will be discussed later in this report.

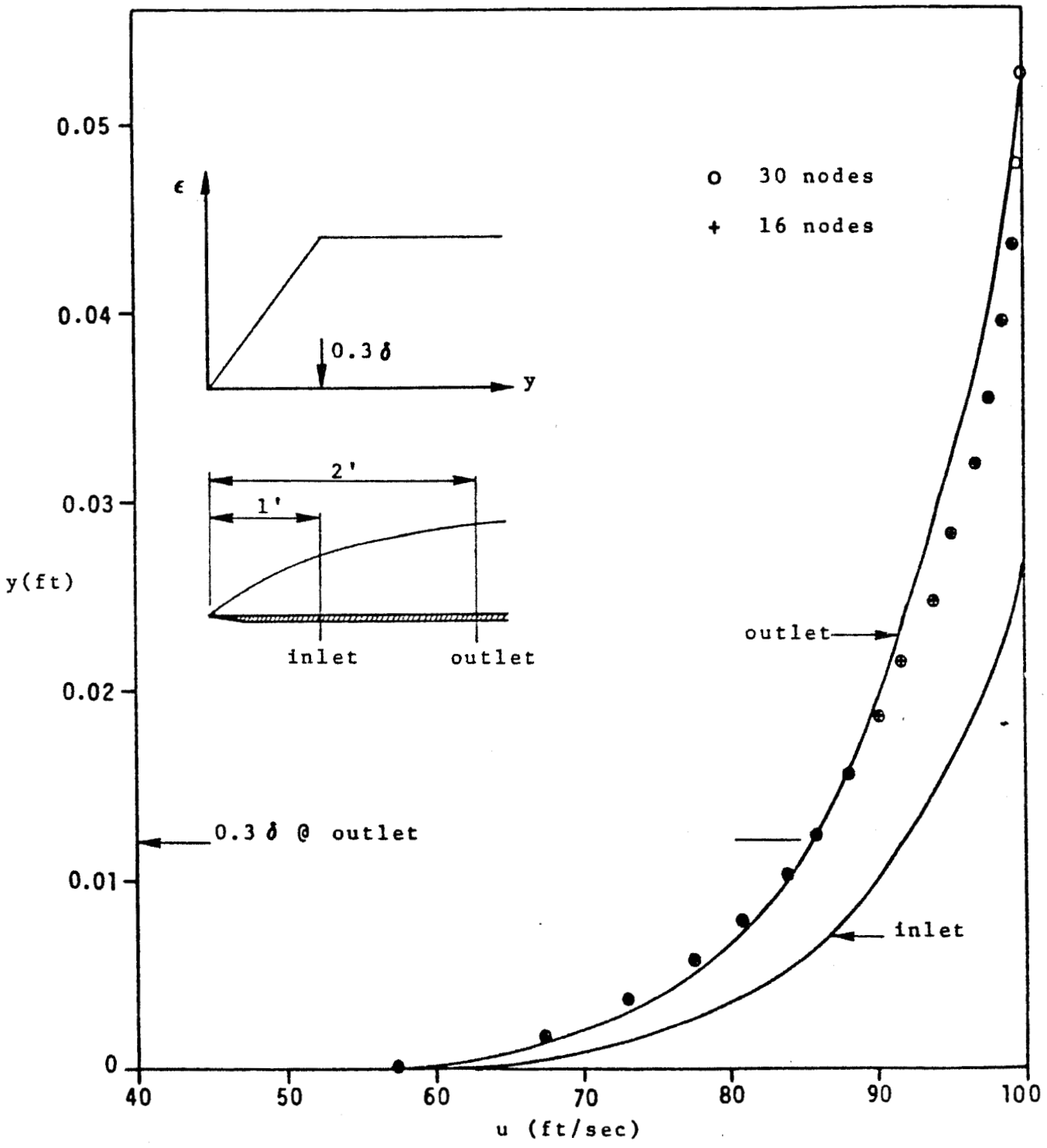

Fig. 13 Turbulent Boundary Layer On A Smooth Flat Plate

Table 2

SHEAR STRESS COMPONENTS

$$\tau_{xx} = 2\mu \frac{\partial u}{\partial x} - \mu_2 \nabla \cdot \bar{V}$$

$$\tau_{yy} = 2\mu \frac{\partial v}{\partial x} - \mu_2 \nabla \cdot \bar{V}$$

$$\tau_{zz} = 2\mu \frac{\partial w}{\partial z} - \mu_2 \nabla \cdot \bar{V}$$

$$\tau_{xy} = \tau_{yx} = \mu \left(\frac{\partial u}{\partial y} + \frac{\partial v}{\partial x} \right)$$

$$\tau_{yz} = \tau_{zy} = \mu \left(\frac{\partial v}{\partial z} + \frac{\partial w}{\partial y} \right)$$

$$\tau_{zx} = \tau_{xz} = \mu \left(\frac{\partial w}{\partial x} + \frac{\partial u}{\partial z} \right)$$

2.4 Turbulent Nozzle Flows

The steady SSME nozzle flow calculations were repeated for turbulent flow with and without heat transfer to the nozzle wall. Turbulent nozzle flows have previously been predicted for the SSME by using the MOC solution and an integral boundary layer treatment (Ref. 5). These predictions show the boundary layer growing from the head end of the chamber, through the throat and along the nozzle wall. With the boundary layer remaining thin in all of these flow passages. The predicted exit plane boundary layer thickness is about 2 in., for both velocity and temperature.

Turbulent flow calculations were made for the SSME nozzle geometry with the mechanical energy and total energy being held constant at all points, except along the wall, for the no-heat transfer case. Exit plane profiles of velocity and temperature are shown in Table 3 for the near wall region. These results show the boundary layer to be thin; the velocity at the wall point is the only point significantly affected by the wall. The distance between the outer two nodes in the exit plane is about 2.5 in.; therefore, the wall point is the only point which should be significantly influenced by wall friction or heat transfer. Two sets of calculations were made for the heat transfer case; the first reset the mechanical energy and total energy at all except the wall points. Table 3 shows that the predictions look good except for the temperature overshoot at the next-to-the-wall point. The second set did not reset the mechanical energy and total energy over the outer 15 percent of the nozzle radius. Table 3 shows that the overshoot is eliminated, but that thickness of both the velocity and thermal boundary layers are overpredicted by this set of calculations. A nozzle wall temperature of 1000°R was used for the heat transfer analyses. Resetting all except the wall points appears to be the best method of performing turbulent flow calculations, but the practice of holding the mechanical energy and total energy fixed requires further examination.

Table 3

TURBULENT NOZZLE EXPANSIONS FOR THE SSME

Radial Position ft	Inviscid Flow q(ft/sec)/T(°R)	Boundary Layer (BL) q(ft/sec/T(°R)	BL w/Heat Transfer* q(ft/sec)/T(°R)	BL w/Heat Transfer ** q(ft/sec)/T(°R)
2.8371	16244/2737	16245/2735	16333/2666	16637/2420
3.0259	16159/2804	16156/2805	16244/2737	16510/2524
3.2146	16038/2899	16040/2898	16123/2832	12249/1039
3.4032	15982/2943	15977/2947	16089/2858	12091/1025
3.5917	15841/3052	15854/3043	15441/3360	12037/1018
3.7801	15808/3078	15742/3047	10066/1339	11989/1014

* Total pressure and energy adjusted at wall only.

** Total pressure and energy adjusted over outer 15% of the flow.

2.5 Three-Dimensional Flows

The VAST code is fully three-dimensional, and all of the methodology discussed to this point is equally applicable to three-dimensional flows. The effect of including the third dimension to the inviscid calculation merely adds the mechanics of solving the third momentum equation. The turbulent flow calculation requires that the distance from the wall be determined for each node point. Such a determination must be made only once for a problem, but the required distances must be stored in an array which is equal in size to the number of nodes used in the problem.

The three-dimensionality of the code has been used extensively in calculating TAD/manifold/transfer duct turbulent flows (Ref. 12). Three-dimensional combustion chamber and nozzle flows have been calculated by Mr. P. Sulyma, (of MSFC) for SRB's. Duplication of axisymmetric calculations have been made; the effect of nozzle cant is still under investigation.

For the SSME, non-uniform flow through the injector face is the major source of three-dimensionality. Parametric analysis of this phenomena is possible with VAST, but calculations for such a flow were not made as a part of this study.

3. TRANSIENT FLOW PREDICTIONS

To describe the transient operation of a liquid-propellant rocket motor, the dynamics of the propellant feed system must be described simultaneously with the flow phenomena in the main combustion chamber and nozzle. Although a great deal is known about the propellant feed systems of operational engines like the SSME, transient simulations of such systems cannot yet be modeled to the extent that local temperatures, pressures and flowrates just upstream of the injector face plates can be predicted. Continuum (Ref. 13) has recently provided an orifice type boundary condition for a combustion chamber which relates local injector mass flowrate to manifold and chamber pressure. Anticipating that better propellant feed system models will be developed, models to represent transient flow in the main combustion chamber will be established.

3.1 Head-End Boundary Conditions

The successful computational anaylsis of the main combustion chamber and nozzle can be conveniently broken into two main topics: (1) the flowfield analog, and (2) the applied boundary conditions. In this section, we will discuss the latter topic and, in particular, the inlet conditions for the motor.

Before discussing the head-end or inlet conditions, let us dispense with all other boundary conditions which are in effect, i.e., the walls and the outlet. The wall boundary conditions are straightforward; involving application of the tangency condition and the shutting off of an unwanted mass, momentum and energy transfer through the solid surface. For curved boundaries application of the tangency condition at the nodes will still lead to apparent flux of conserved quantities through the walls. This tendancy is eliminated by discarding the apparent flux through the wall in the element integral calculation. It is also possible to achieve flux cancellation by defining the local tangency as the chord slope between the surrounding node points. This approach was discarded since the local flow angle definition becomes grid dependent.

The outlet boundary condition is more complex. If the steady state operating condition is all that is desired and the nozzle flow is supersonic then no boundary conditions, or one-sided differencing, are adequate treatments of the outlet. In the early stages of start-up

and during shut-down, the surrounding atmosphere must be included in the analysis. That is to say that the applied boundary condition is far removed from the nozzle exit plane, rather than at the exit plane.

If enough surrounding atmosphere is included in the analysis, then the downstream boundary condition becomes simply those atmospheric conditions which exist at the edges of the computational region during the start-up transient. During shut-down (since the plume is very long), a twofold strategy becomes necessary. During the early stages of shut-down, the plume penetrates the downstream boundary and, as the exhaust gas production declines, the plume collapses and atmospheric air moves in to occupy the void. Initially then, the steady state plume drives the downstream boundary and the condition used is free. After the plume has collapsed, however, we must return to the atmospheric definition. This process has not been automated and currently is left to the judgment of the investigator.

During the start-up transient, we must define a sufficiently large atmospheric region around the exit plane of the nozzle that simply allows the edges to be free. After the nozzle is flowing full, then the region under investigation may be reduced to simply the nozzle itself.

Having dispensed with the relatively straightforward wall and outer boundary conditions, we now turn our attention to the inlet or head-end conditions. To provide ultra-realistic transients, it is necessary to model the engine upstream of the combustor to some deg.. Usually this is so complex that one must settle for a simplified expression for the manifold pressure upstream of the injectors. A candidate approach is to specify the total pressure and total temperature downstream of the injectors. If prior testing has yielded a head-end static pressure (which is generally assumed to be the total pressure, since the kinetic energy of the propellants is usually negligible), then this information along with an estimated flame temperature is adequate to perform an analysis of the combustor and nozzle. This is particularly true at steady state.

All three options are available in the VAST analysis:

- Analyze in detail the upstream components of the motor.
- Use manifold conditions and approximate orifice pressure drops.
- Use known conditions downstream of the injector.

In the latter two cases, the VAST codes calculate the motion of the independent variables at the head-end edge of the computational region. Retaining the instantaneously local value of the pressure (actually, any state variable can be used) and the instantaneous flow angle, all other required variables can be calculated to enforce the required condition.

The condition of known total pressure and total temperature downstream of the injector is then treated in the following fashion:

1. The quantities at each mode of the upstream edge of the computational zone are computed at the end of the nth time step. They are ρ^n, ρu^n, ρv^n, ρE^n and from these properties the pressure p^n is computed.

2. The local flow angle (two-dimensional only is shown for explanatory purposes) is computed as $\theta = \tan^{-1} (\rho v^n / \rho u^n)$

3. From the known total conditions and the local instantaneous pressure, compute new values of the primary variables:

$$\hat{\rho}^n = \rho_o \ (p^n/p_o)^{(1/\gamma)}$$

$$\hat{T}^n = p^n/(\hat{\rho}^n R)$$

$$\rho \hat{u}^n = \hat{\rho}^n \sqrt{2C_p(T_o - \hat{T}^n)} \ \cos\theta$$

$$\rho \hat{v}^n = \hat{\rho}^n \sqrt{2C_p(T_o - \hat{T}^n)} \ \sin\theta$$

$$\hat{\rho} E^n = \hat{p}^n/(\gamma-1) + \frac{\left[(\rho \hat{u}^n)^2 + (\rho \hat{v}^n)^2 \right]}{2\hat{\rho}^n}$$

Where the symbol (^) denotes the adjusted value.

The first two steps are identical where the manifold/orifice boundary condition is involved. The steps to compute the adjusted conditions are altered, however. They are:

$$\hat{\rho} q^n = C_I \sqrt{2\rho_o (p_o - p^n)} \; / \; S_c$$

$\hat{\rho}^n$, $\rho \hat{E}^n$ are known input values.

And where C_I is the local effective discharge coefficient and S_c is the local orifice flow area locally.

One additional boundary condition is implicit in the analysis at the throat through the choking condition. The condition, which corresponds to the maximum mass flow which the nozzle can pass (at a given initial condition), occurs automatically in the solution of the field. Once this occurs, the chamber is no longer sensitive to the downstream boundary condition at the exit of the nozzle, or to any changes in the external field.

These, then, are the conditions which are available and, indeed, must be used to provide a realistic start-up transient and steady state solution, as well as the shut-down transient, if desired. It should be pointed out that the head-end conditions may be provided as a function of time making the entire unsteady solution as good as the known head-end information.

3.2 Rapid Start-up and Shut-down Transients

For an ideal gas simulation of parallel flow in a cylindrical combustion chamber, the total conditions and one additional variable must be specified. For steady flow, the additional variable is determined by the choking condition at the throat to evaluate the mass flowrate. In the transient solution, however, the mass flowrate of each cross section is different. At very early times, for instance, there is flow into the chamber but no flow through the throat. For liquid-propellant motors, the model postulated in this analysis is that the total pressure, total temperature, flow angle and static pressure at

the injector are specified functions of time. Continuum has previously reported a solution obtained in this manner to simulate a J-2S (Ref. 14). Since only the methodology was demonstrated in that work, unrealistically fast start-up transients were simulated in order to foreshorten the calculations.

3.3 Slow Start-up and Shut-down Transients

Since the pressure rise rates in the SSME are very low, a series of steady-state solutions at intermediate pressure levels will adequately describe the nozzle flow. Again, precautions to apply downstream boundary conditions well away from the computational region of interest must be exercised. The codes and procedure for this calculation have been developed but the actual calculations have not been performed. Calculations for a STAR 48 nozzle have been conducted and are shown in Fig. 14. Notice the large Mach disc which is predicted.

STAR48 FAILURE ANALYSIS

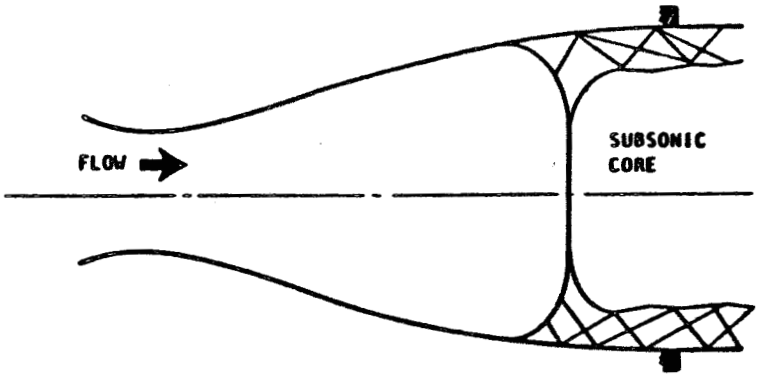

RESTRICTED SHOCK SEPARATION

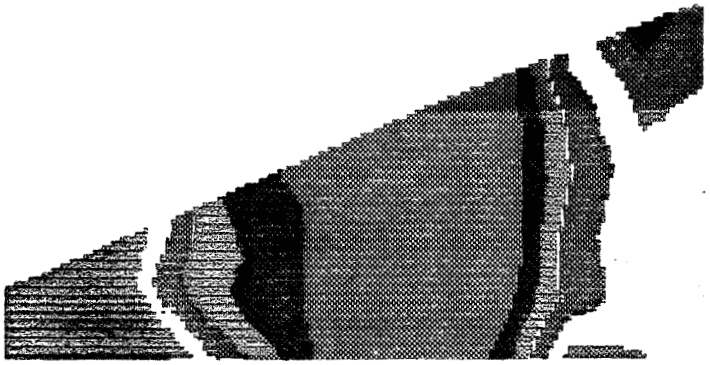

STATIC PRESSURE AT .23 SECONDS (PC=150 PSIA)

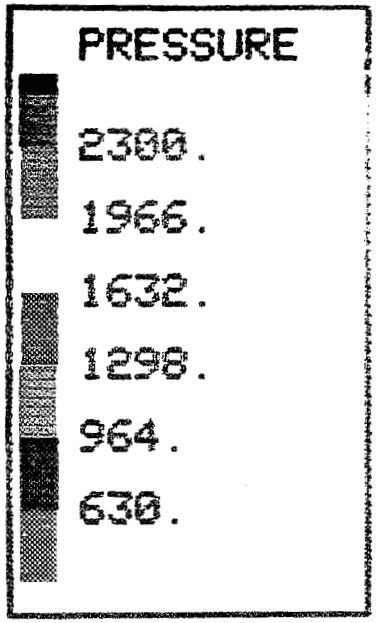

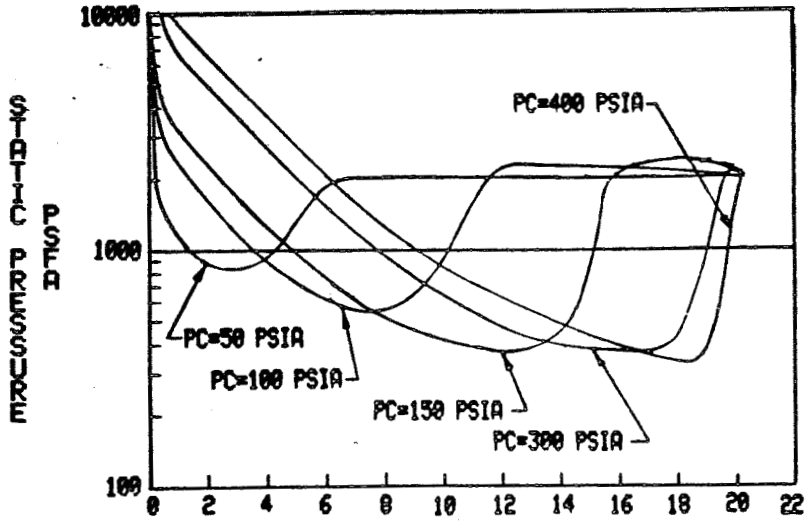

CALCULATED NOZZLE WALL STATIC PRESSURE DISTRIBUTION

ORIGINAL PAGE
COLOR PHOTOGRAPH

Fig. 14 STAR48 Nozzle Analysis

4. CONCLUSIONS

A transient, axisymmetric, two-dimensional and three-dimensional CFD analysis for the SSME main combustion chamber and nozzle flow was developed. Viscous/turbulence models were included in the analysis.

A critical feature of CFD methods for nozzle flow with large expansions is the accuracy with which total pressure is determined. Any CFD method considered for use in modeling nozzle expansions should be carefully evaluated to determine how accurately total pressure is predicted. The VAST code with the discussed constraints accurately predicts total pressure.

Turbulent momentum and heat exchange at the system walls are accurately predicted with the VAST code. Thermal and momentum boundary layer thicknesses compare well with MOC/boundary layer models.

Further investigations need to be made to determine the local flow rates through injectors and the transient head-end boundary conditions appropriate to describing SSME flows.

5. REFERENCES

1. Farmer, R.C., R.J. Prozan, L.R. McGimsey, A.W. Ratliff, "The Verification of a Mathematical Model which Represents Large, Liquid Rocket Engine Plumes", AIAA Paper No. 66-650 (June 1966).

2. Pieper, J.L., "Performance Evaluation Methods for Liquid Rocket Thrust Chambers", Aeroject Co., Report TCER9642:0067 (September 1966).

3. Prozan, R.J., "Hypothesis of a Variational Principle for Compressible Fluid Mechanics", CI-TR-0086 (March 1985).

4. Back, L., AIAAJ, 4, pp. 2219-2221 (December 1966).

5. Evans, R.M., "Boundary Layer Integral Matrix Procedure", Aerotherm Corp., UM-75-64 (July 1975).

6. Chan, J.S. and J.A. Freeman, "Throat Chamber Performance using Navier-Stokes Solution", Lockheed R & D Div, HREC, LMSC-HREC-TRD951729 (December 1984).

7. Przekwas, A.J., A.K. Singhal, L.T. Tam, "SSME Thrust Chamber Simulation using Navier-Stokes Equations", CHAM, Inc. CHAM 40703 (October 1984).

8. Cebeci, T. and A.M.O. Smith, Analysis of Turbulent Boundary Layers, Academic Press, NY (1974).

9. Hinze, J.D., Turbulence, 2nd ed, McGraw-Hill, NY (1975).

10. Schlichting, H., Boundary Layer Theory, 7th ed, McGraw-Hill, NY (1979).

11. Weigand, G.G. and J.D.A. Walker, in Turbulent Boundary Layers, H.E. Weber, ed, ASME, NY, pp. 221-235 (June 1979).

12. Anderson, P.G. and R.C. Farmer, "Calculation of Flow About Posts and Powerhead Model", Continuum, Inc., Interim Report on NAS8-35506 (December 1985).

13. Wang, T.S. and R.C. Farmer, "Computational Analysis of the SSME Fuel Preburner Flow", Continuum, Inc., CI-FR-0084 (February 1986).

14. Farmer, R.C., "Ignition and Combustion Processes: Development of A Transient, Three-Dimensional Rocket Engine Analysis", Continuum, Inc., Contract NAS8-35260 (June 1984).